THE AMERICAN SOCIETY OF MECHANICAL ENGINEERS
Three Park Avenue, New York, N.Y. 10016-5990

99-GT-108

EXPERIMENTAL AND NUMERICAL STUDIES OF TWO-STAGE ETHANE-AIR FLAMES

M.M.Y. Waly, S.C. Li and F.A. Williams

Center for Energy and Combustion Research
Department of Applied Mechanics and Engineering Sciences
University of California, San Diego
La Jolla, CA 92093-0411

Presented at the International Gas Turbine & Aeroengine Congress & Exhibition
Indianapolis, Indiana — June 7–June 10, 1999
This paper has been accepted for publication in the Transactions of the ASME
Discussion of it will be accepted at ASME Headquarters until September 30, 1999

ABSTRACT

This paper reports results of experimental and numerical investigations on ethane-air two-stage combustion in a counterflow burner where the fuel stream, which is partially premixed with air for equivalence ratios from 1.6 to 3.0, flows against a pure air stream. Similar to methane, the two-stage ethane combustion exhibits a green fuel-rich premixed flame and a blue diffusion flame. Flame structures, including concentration profiles of stable intermediate species such as C_2H_4, C_2H_2 and CH_4, are measured by a gas chromatography and are calculated by numerical integrations of the conservation equations employing an updated elementary chemical-kinetic data base. The implications of the results from these experimental measurements and numerical predictions are summarized, the flame chemistry of ethane two-stage combustion at different degrees of premixing (or equivalence ratio) is discussed, and the relationship between NOx formation and the degree of premixing is established. The present work helps to increase understanding of flame chemistry of hydrocarbon fuels, identify important reactions for pollutant formation and suggest means to reduce emissions.

INTRODUCTION

Ethane is the second most important hydrocarbon constituent of natural gas (NG). Variation of ethane concentration is found to influence ignition, combustion and extinction of NG-air mixtures in practical applications such as in gas turbines and internal combustion engines [1]. Trumpy et al. [2] and Leppard [3] studied preknock chemistry of ethane in internal combustion engines and helped to develop understanding of the ethane ignition mechanism at temperatures lower than 1100 K. Laurendeau and coworkers developed an experimental method using laser-saturated fluorescence to measure nitric oxide in laminar $C_2H_6/O_2/N_2$ premixed flames [4] and in laminar counterflow ethane diffusion flames [5]. These nonintrusive optical measurements of NO have advanced our knowledge on NO formation in both premixed and diffusion flames. Lean premixed flames of ethane at pressures ranging from 1 to 10 atm were studied by Drake et al [6] in a flat-flame burner, providing useful information to better understand NO production at high pressures.

Detailed measurements and computations for flame structures of staged ethane combustion are not available in the literature. Since those measurements and their comparison with theory may improve our understanding of two-stage ethane flame chemistry in gas turbines and other combustors, an experimental and computational study of a two-stage ethane-air flame is performed here to investigate how ethane is oxidized and how the intermediate species such as C_2H_4, C_2H_2 and CH_4 are formed in rich premixed and diffusion flames. As, discussed in our previous publications [7, 8], staged combustion can be realized in a counterflow burner where, for instance, a fuel-rich mixture flows downward counter to a stream of pure air.

A practical motivation for studying this configuration arises from its possible utility in increasing combustion stability and combustion efficiency and in reducing pollutants. A test rig can be constructed that affords ready access for instrumentation, and complementary theoretical and computational studies are facilitated by reduction of the applicable conservation equations along the centerline to ordinary differential equations.

EXPERIMENT

This study employed a laminar counterflow burner which is schematically shown in Fig. 1(a). In this burner, coaxial streams issue from two ducts placed one above the other, each with exit inner diameter of 20 mm. The separation distance between the duct exits is $L = 15$ mm. The ethane-air mixture flows through the upper duct, and the pure air stream flows through the lower duct. The equivalence ratio of the fuel stream is in the range from 1.6 to 3.0 in the present study while the mean strain rate in the oxidizer stream is adjusted to be around 90 s^{-1} based on the total flow rates from the upper duct and from the lower duct.

In the experiment, the desired equivalence ratio and strain rate are established first, and then a torch is used to ignite the flame. A typical photograph of such a flame is shown in Fig. 1(b). It can be seen that there are two distinguished flame zones: One is thin with green emission, and the other is thicker with blue emission. The former is the premixed flame, where the ethane is consumed to form carbon monoxide and hydrogen along with

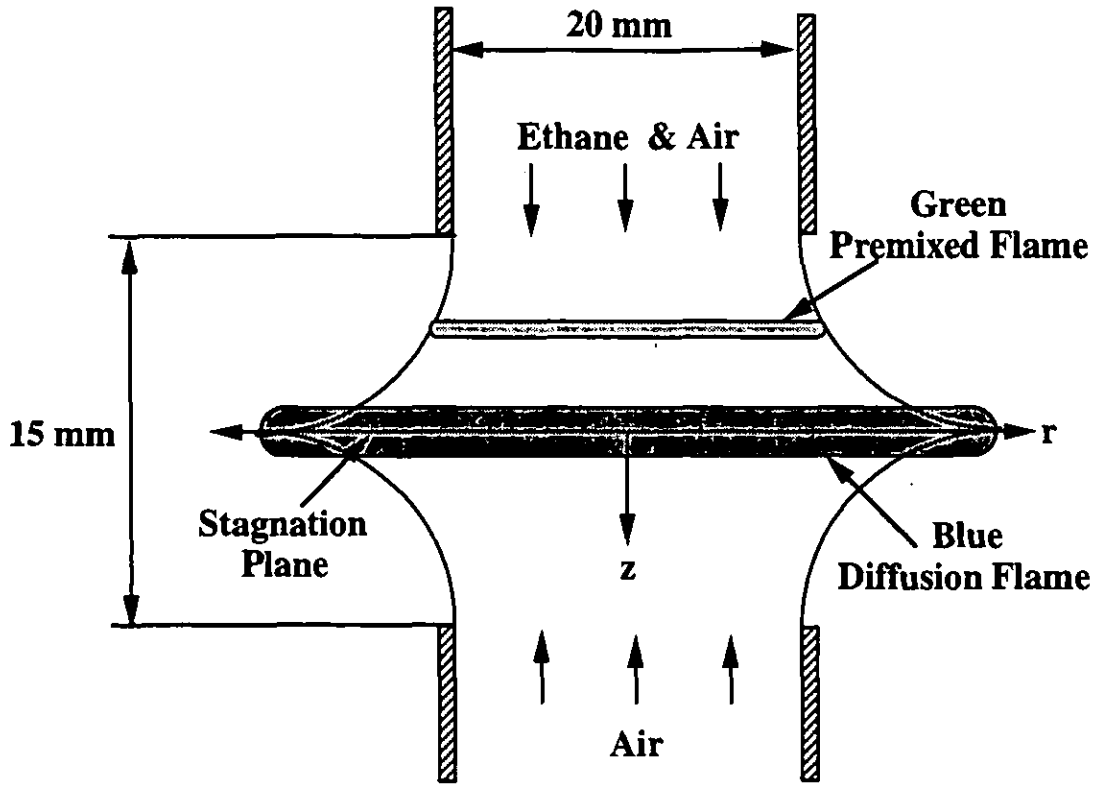

Fig.1a: Schematic diagram of a two-stage flame of ethane in counterflowing streams.

Fig.1b: A photograph of the flame sketched above.

some carbon dioxide and water, and the latter is the diffusion flame, where the CO and H_2 produced in the first stage burn. It seems likely that the color of the premixed flame is dominated by emissions from C_2 species, while that of the diffusion flame reflects excited CO_2 emissions stemming from the oxidation of CO. These flame colors are the same as those of two-stage methane-air flames [7].

A SRI-8610C gas chromatograph (SRI Instruments), which has Molecular Sieve and Silica Gel columns with a thermal conductivity detector (TCD) and a flame ionization detector (FID), is employed to measure concentrations of stable species. A methanizer accessory is built in the gas chromatograph so that the FID can be used to measure concentrations of CO and CO_2 as well as those of hydrocarbon species. Gas samples in the flame are taken by a quartz microprobe whose tip has a outer diameter around 0.5 mm and an inner diameter around 0.1 mm. In the present ethane flames, the measurable species by the FID are CH_4, CO, CO_2, C_2H_6, C_2H_4, C_2H_2 and C_3H_6. Nitrogen and oxygen are measured by the TCD. Concentrations of water and hydrogen are not measured in the present study. Temperature profiles are measured with a Pt-6%Rh vs. Pt-30%Rh thermocouple with a bead diameter of 140 μm; corrections for radiation are made. The accuracy of measurements for temperature and species was discussed in our previous studies [7, 8].

NUMERICAL COMPUTATIONS

The computational methods employed here were described previously [7, 8]. The numerical integrations concern laminar flames with potential flow in the outer streams. Radiation from CO_2 and H_2O is taken into account in the energy equation. With these assumptions, the equations of continuity, radial momentum, energy and chemical species reduce to those given previously [9, 10]. The present computations employ a numerical code developed at RWTH, Aachen, Germany [11].

The present study employs a detailed chemical mechanism consisting of 186 elementary reactions among 45 species, which are CH_3O, CH_2OH, O_2, H_2, H_2O, HO_2, H_2O_2, H, OH, O, CO, CO_2, CH_4, CH_3, CH_2O, CHO, C_2H_6, C_2H_5, C_2H_4, C_2H_3, C_2H_2, C_2H, singlet $^*CH_2$ and triplet CH_2, CH, HCCO, C_3H_7, C_3H_6, C_3H_5, C_3H_4, C_3H_3, N_2, HCN, N, NH_3, NH_2, NH, HNO, NO, N_2O, N_2H, NO_2, NCO, CN and HNCO. This reaction mechanism is upgraded from our 177-step reaction mechanism [8] by adding species C_2H and 9 reactions for its production and consumption. These 9 reactions and their rate parameters for C_2H are taken from the paper by Frenklach et al. [12] (reactions 95-101, 107 and 111). With the exception of the rate parameters for $C_2H_4 + H \rightarrow C_2H_3 + H_2$ and $C_2H_4 + OH \rightarrow C_2H_3 + H_2O$ as discussed below, all rate parameters listed in Table 1 of [8] are kept unchanged in the present study.

RESULTS OF EXPERIMENTAL MEASUREMENT AND NUMERICAL COMPUTATION

The computational results are compared with the measurements in Figs. 2 through 6, and predicted NO, CH, N and HCN are shown in Fig. 7. Each one of these figures has four subfigures, labeled (a), (b), (c) and (d), which correspond to equivalence ratios of 1.65, 1.85, 2.20 and 2.65, respectively, in decreasing degree of premixing. Results in these figures show how the equivalence ratio or the degree of premixing influences structures of ethane flames. In the following, flame structures, signified by the profiles of CO, CO_2 and temperature, will be discussed first. Ethane consumption chemistry will be analyred second. Next the formation and consumption chemistry of intermediate species C_2H_4, C_2H_2 and CH_4 in two-stage ethane flames will be discussed. Finally, the implication concerning NOx formation will be summarized. Discussions of C_3 species, such as C_3H_6, are not included here since their concentrations are negligibly low compared with the intermediate species mentioned above.

Structures of Two-Stage Ethane Flames

Figure 2 shows profiles of temperature T and of concentrations of reactants C_2H_6 and O_2 and products H_2, CO and CO_2, indicating good agreement of measured and predicted profiles for CO, CO_2 and temperature, T, differences typically being less than 10%; comparable with the previously discussed [7, 8] measurement uncertainty. The two-stage structure is very evident at the higher degrees of premixing in Fig. 2(a) and (b), with the premixed flame on the left, producing CO and H_2, which burn with O_2 from the air in the diffusion flame about 4 mm away. At the lesser premixing in Fig. 2(c) and (d) the two flames have nearly merged, so that CO peaks only slightly to the left of CO_2. This can be understood easily by referring to Fig. 1 where the configuration illustrates that the premixed flames with lower equivalence ratios have higher burning velocities and propagate further upstream, producing larger separation distances between the two flames. Increasing the strain strain rate slightly decreases the separation distance but does not change the flame structure.

The maximum CO concentration occurs in the premixed flame, while the maximum concentration of CO_2 can be found in the diffusion flames. As expected, Fig.2 shows that the maximum concentration of CO decreases with increasing equivalence ratio; experiment and computation agree, although spatial resolution difficulties prevent experimental identification of the peak value at the higher Φ values. The maximum concentration of CO_2 is essentially the same for different premixing and, consequently, the maximum flame temperature is about 2100 K for all four cases, regardless of equivalence ratio. This is because all of the fuel is burned completely in the two-stage combustion at the same strain rate.

The production and oxidation of CO are found to occur

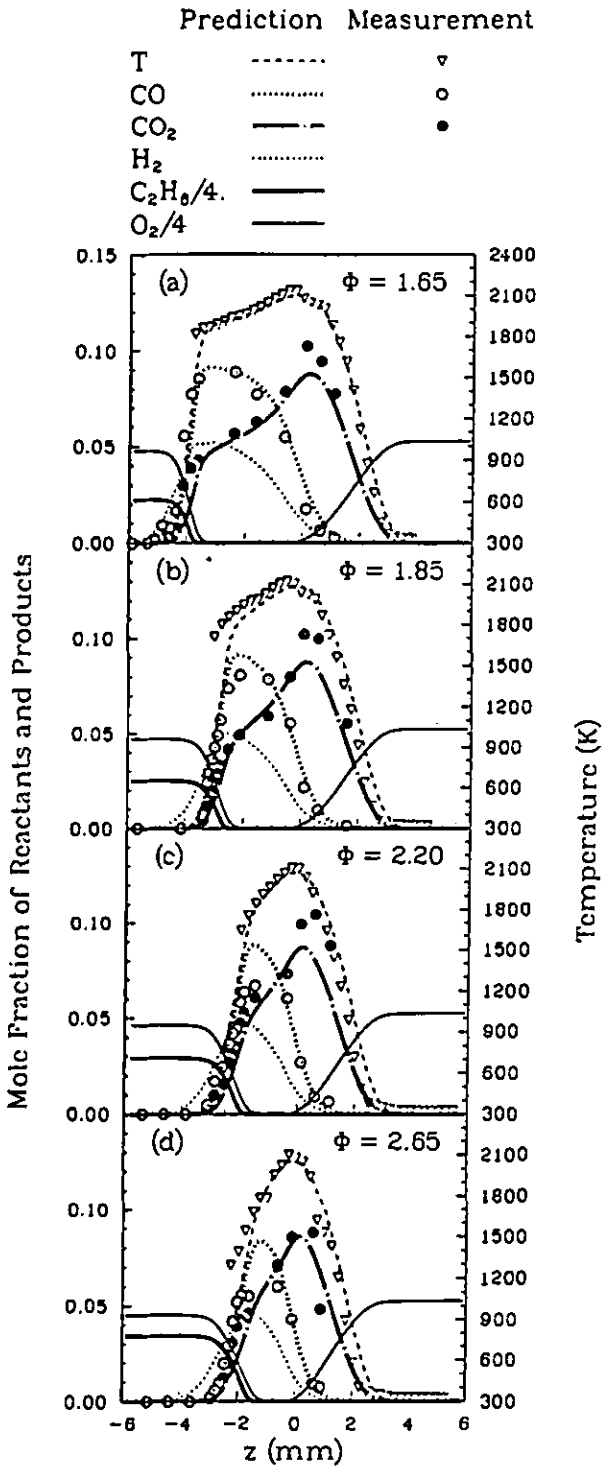

Figure 2: Comparison between measurement and prediction for profiles of temperature and major species for strain rate $a = 90$ s^{-1} at different equivalence ratios: (a) $\Phi = 1.65$; (b) $\Phi = 1.85$; (c) $\Phi = 2.20$; (d) $\Phi = 2.65$.

mainly through the reactions

$$CHO + M \rightarrow CO + H + M \quad (R1)$$

$$CH_2 + O_2 \rightarrow CO + OH + H \quad (R2)$$

$$HCCO + H \rightarrow CO + {}^{\bullet}CH_2 \quad (R3)$$

$$HCCO + O_2 \rightarrow 2CO + OH \quad (R4)$$

and

$$CO + OH \rightarrow CO_2 + H. \quad (R5)$$

These reactions are consistent with CO being produced in the premixed flame, since CHO, CH_2 and HCCO are formed and consumed there and do not exist in the diffusion flame as shown in the analysis. Through reaction R5, most of CO_2 is formed in the diffusion flame in which the OH concentration peaks and in which the CO concentrations are everywhere much higher than those of OH and thus the CO is consumed in a distributed reaction zone.

Ethane Consumption Chemistry

Figures 3 shows measured and predicted profiles of ethane concentrations. Computed concentrations of the radicals H, OH and O are also plotted in this figure since these radicals are the dominant species that attack ethane and other hydrocarbon fuels. For orientation, predicted profiles of temperature are replotted in Fig. 3 to show the relationship between the two-stage flame and species concentrations. It is seen that ethane rapidly disappears in the premixed-flame reaction zone where the temperatures are around 1750 K.

The four principal reactions that consume ethane, identified by the numerical computations, are

$$C_2H_6 + H \rightarrow C_2H_5 + H_2 \quad (R6)$$

$$C_2H_6 + O \rightarrow C_2H_5 + OH \quad (R7)$$

$$C_2H_6 + OH \rightarrow C_2H_5 + H_2O \quad (R8)$$

and

$$C_2H_6 + CH_3 \rightarrow C_2H_5 + CH_4. \quad (R9)$$

At low equivalence ratios, two peaks are predicted in the H and OH concentration profiles, a low peak in the premixed flame and a much higher peak in the diffusion flame. Concentrations of OH in the premixed flames are much lower than those of H, and reaction rates of R6 are much faster than those of R7, R8 and R9, based on computational results. Therefore, about 80% of ethane is consumed by Reaction R6. From Fig. 3, it is also seen that the radical H, which is produced in the premixed flame, diffuses back to attack the reactants.

The ethyl radical C_2H_5, which is unstable, decomposes rapidly to C_2H_4 and CH_3 through reactions

$$C_2H_5 + M \rightarrow C_2H_4 + H + M, \quad (R10)$$

$$C_2H_5 + H \rightarrow 2CH_3 \quad (R11)$$

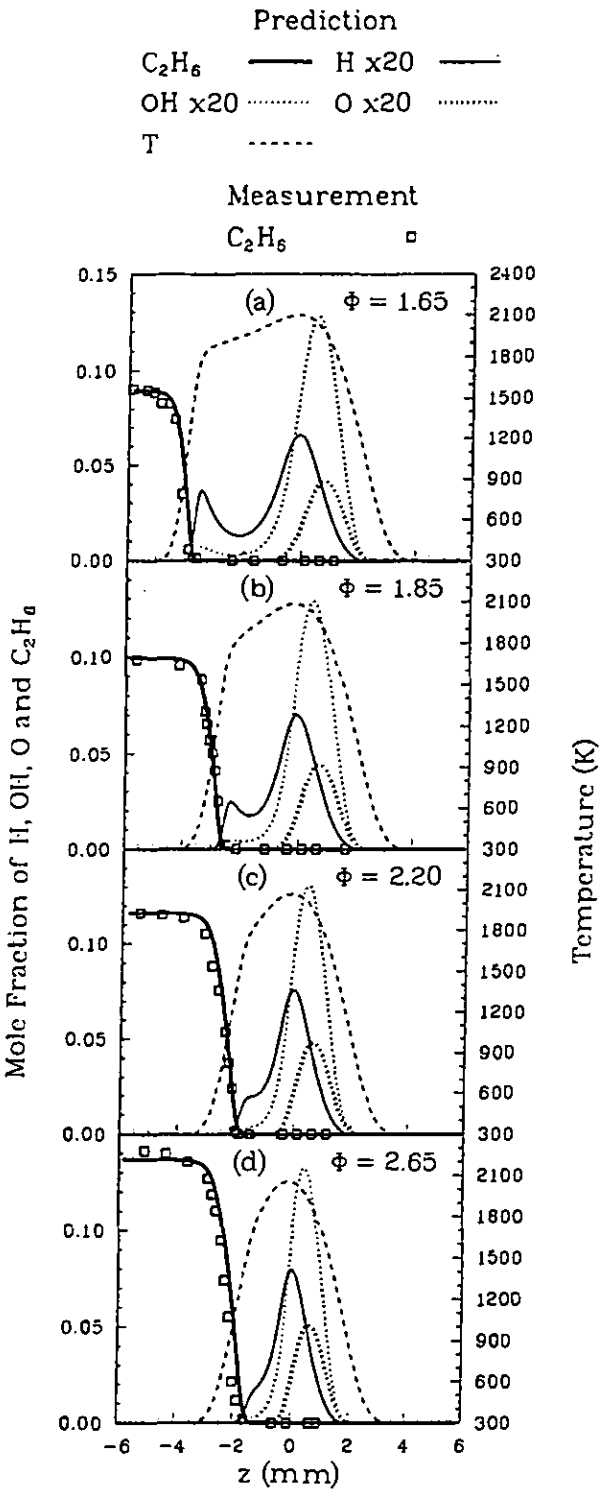

Figure 3: Comparison between measurement and prediction for concentration profiles of ethane and predicted concentration profiles of radicals H, OH and O for strain rate $a = 90\ s^{-1}$ at different equivalence ratios: (a) $\Phi = 1.65$; (b) $\Phi = 1.85$; (c) $\Phi = 2.20$; (d) $\Phi = 2.65$.

and

$$C_2H_5 + O_2 \rightarrow C_2H_4 + HO_2. \qquad (R12)$$

Reactions R10 and R11 consume more than 60% and 30% of C_2H_5, respectively. It should be noted that reactions R1, R2, R5 and R10 are the major sources of H radicals in the premixed-flame reaction zone. The main products from reactions R6 through R12 are H_2O, H_2, C_2H_4, CH_4 and CH_3, with the latter four species being further oxidized.

Formation and Consumption of CH_4

Measured and predicted profiles of CH_4 concentrations are plotted in Figs. 4(a)-(d). These figures indicate that the maximum mole fraction of CH_4 is about 0.5% and is insensitive to the equivalence ratio in these two-stage ethane flames. The CH_4 is formed dominantly by

$$CH_3 + H \rightarrow CH_4 \qquad (R13)$$

and by reaction R9. The CH_4 is consumed by the three well-known reactions

$$CH_4 + H \rightarrow CH_3 + H_2, \qquad (R14)$$

$$CH_4 + OH \rightarrow CH_3 + H_2O \qquad (R15)$$

and

$$CH_4 + O \rightarrow CH_3 + OH. \qquad (R16)$$

As shown in Fig. 4, good agreement between experiment and prediction can be obtained by using the rate parameters of reactions R6 through R15 which are listed in the Table 1 of [8]. All of the differences seen in Fig. 4 can be attributed to uncertainties in probe positioning and sampling.

C_2H_4 Chemistry

The C_2H_4 is consumed by the reactions

$$C_2H_4 + H \rightarrow C_2H_3 + H_2, \qquad (R17)$$

$$C_2H_4 + O \rightarrow CH_3 + CHO \qquad (R18)$$

and

$$C_2H_4 + OH \rightarrow C_2H_3 + H_2O. \qquad (R19)$$

Among these three reactions, reaction R17 consumes most of the C_2H_4. This occurs because the concentration of H is much larger than that of the O and OH in the premixed flame zone, as shown in Fig. 5, and computations show that reaction rates of R17 are much higher than those of R18 and R19 there.

By neglecting less important reactions, a chemical-kinetic-steady state balance for the C_2H_5 and C_2H_4 species results approximately in

$$X_{C_2H_4} \approx \frac{k_6 X_{C_2H_6} X_H}{(k_{17} X_H + k_{19} X_{OH})(1 + k_{11} X_H / k_{10})} \qquad (1)$$

where k_i is the rate constant of the reaction Ri and X denotes the mole fraction of the species. It is found that if the rate parameters listed in [8] are used, then the predicted concentration

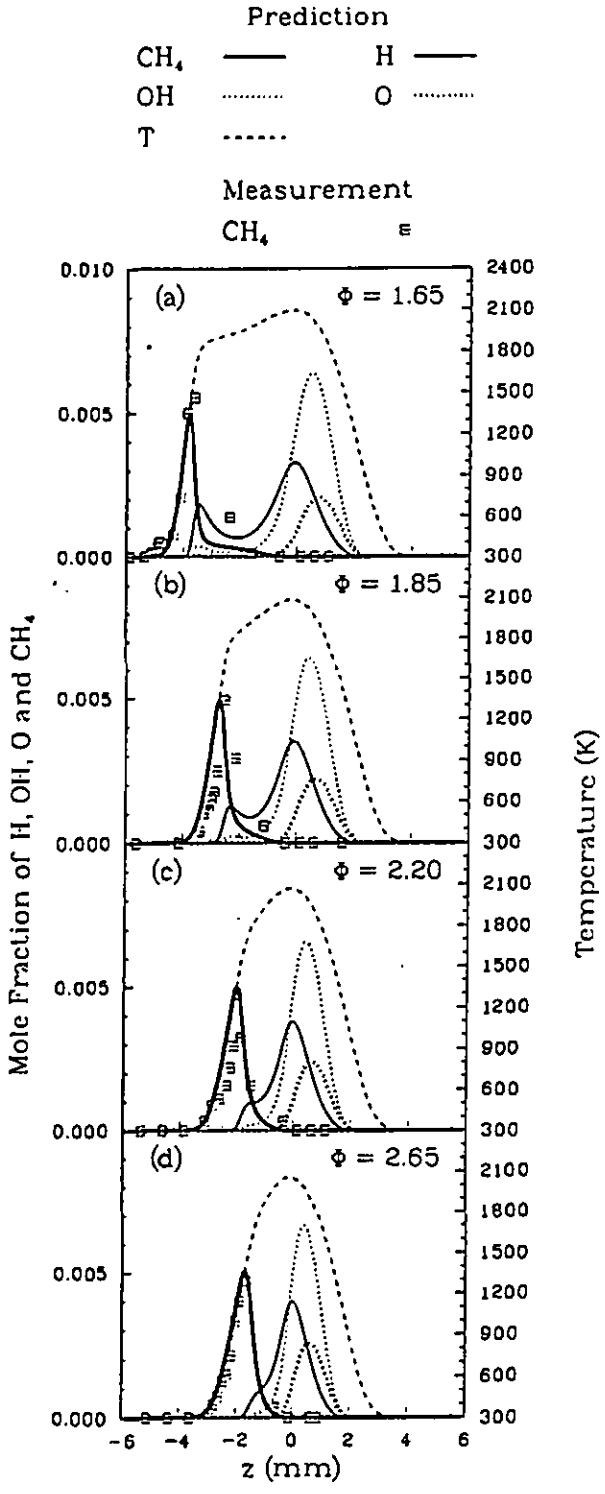

Figure 4: Comparison between measurement and prediction for concentration profiles of intermediate species CH_4 and computed concentration profiles of radicals H, OH and O for strain rate a = 90 s^{-1} at different equivalence ratios: (a) Φ = 1.65; (b) Φ = 1.85; (c) Φ = 2.20; (d) Φ = 2.65.

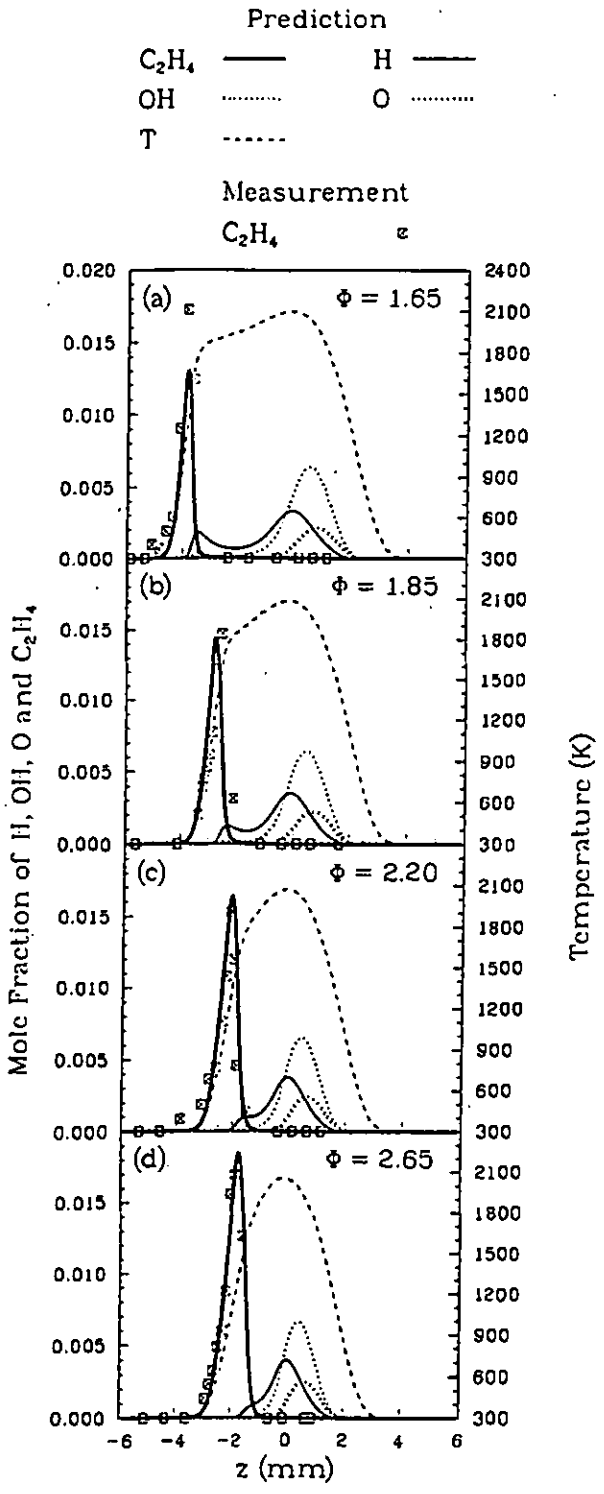

Figure 5: Comparison between measurement and prediction for concentration profiles of intermediate species C_2H_4 and computed concentration profiles of radicals H, OH and O for strain rate a = 90 s^{-1} at different equivalence ratios: (a) Φ = 1.65; (b) Φ = 1.85; (c) Φ = 2.20; (d) Φ = 2.65.

of C_2H_4 is too low by a factor of two, while the sum of the concentrations of C_2H_2 and C_2H_4 is too high in comparison with experimental results. This problem was not encountered in our previous work [8] because concentrations of both C_2H_4 and C_2H_2 are much lower in methane flames than in ethane flames and because C_2H_4 and C_2H_2 were not distinguishable by the Porapak Q column used in the previous gas chromotogrph measurements [8].

According to Eq. 1, the concentration of C_2H_4 increases with increasing k_6 and with decreasing k_{17}, k_{19} and k_{11}/k_{10}. The values of k_6, k_{10} and k_{11}, however, cannot be changed because these values are less uncertain and have led to the good agreements as shown in Figs. 3- 4, for example. In order to obtain improved agreements between measured and predicted concentrations of both C_2H_4 and C_2H_2, values of k_{17} and k_{19} are reduced to $k_{17} = 2.25\times10^7 T^{2.12}\exp(-6727/T)$ and $k_{19} = 2.70\times10^5 T^{2.31}\exp(-1450/T)$, respectively, which are smaller by a factor of 2 than those given by Bhargava and Westmoreland [13]. These new rate constants are within the reported [13] uncertainties, which are a factor of 2.4 in k_{17} and a factor of 2.75 in k_{19}.

Figures 5(a)-(d) compare measured concentrations of C_2H_4 with predictions based on these new rate constants k_{17} and k_{19}. It is seen that the agreements are excellent. These figures indicate that the maximum concentration of C_2H_4 increases with increasing equivalence ratio as the premixed flame (shown in Fig. 1b), where C_2H_4 disappears, moves closer to the stagnation plane located at $x = 0$.

Formation and consumption of C_2H_2

The radical C_2H_3, which is the main product of reactions R17 through R19, decomposes to C_2H_2 dominantly by

$$C_2H_3 + M \rightarrow C_2H_2 + H + M \qquad (R20)$$

and less importantly by

$$C_2H_3 + H \rightarrow C_2H_2 + H_2 \qquad (R21)$$

and

$$C_2H_3 + O_2 \rightarrow C_2H_2 + HO_2. \qquad (R22)$$

Following these reactions, the C_2H_2 is oxidized mainly by

$$C_2H_2 + O \rightarrow HCCO + H \qquad (R23)$$

and

$$C_2H_2 + O \rightarrow CH_2 + CO. \qquad (R24)$$

Different from CH_4, C_2H_4 and C_2H_6, which are mainly attacked by the H radical, the removal of C_2H_2 is dominantly by the O radical in the current reaction scheme. In a first approximation, a chemical-kinetic steady-state balance for C_2H_2 results in

$$X_{C_2H_2} \approx \frac{k_{17} X_{C_2H_4} X_H}{(k_{23} + k_{24}) X_O}. \qquad (2)$$

This equation implies that the lower consumption rate of C_2H_4 leads to a lower concentration of C_2H_2 in the flame, consistent

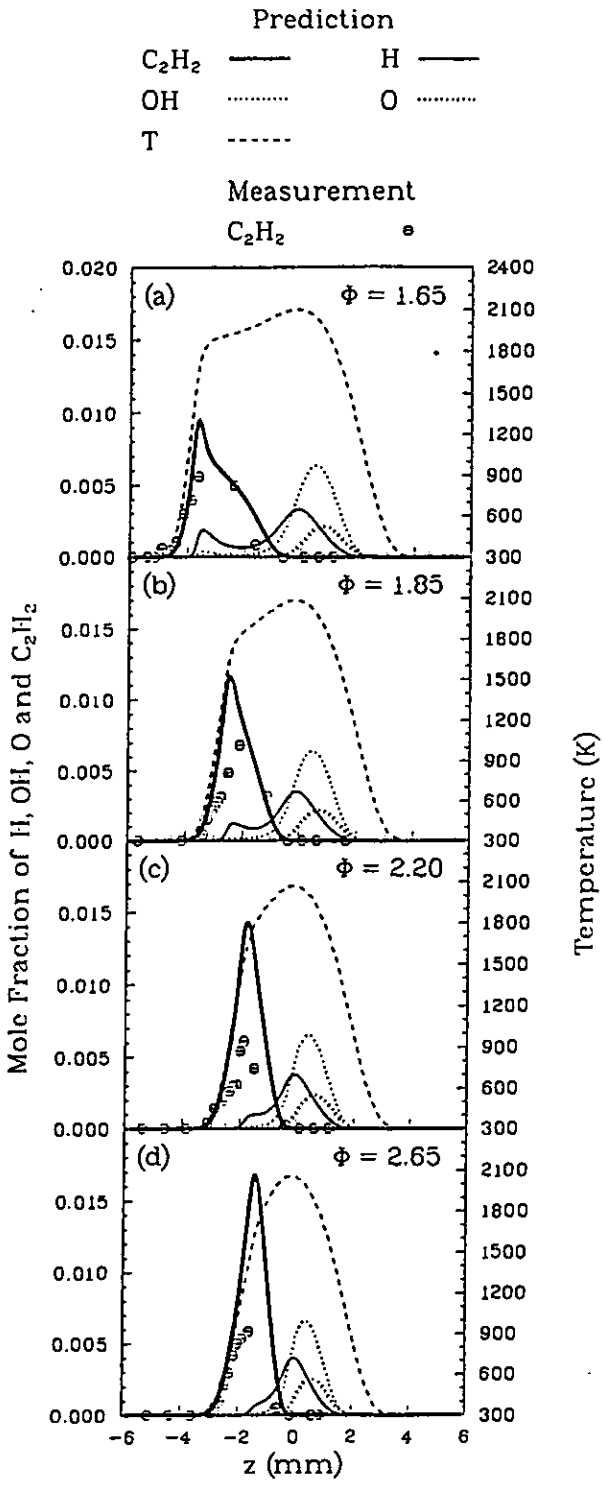

Figure 6: Comparison between measurement and prediction for concentration profiles of intermediate species C_2H_2 and computed concentration profiles of radicals H, OH and O for strain rate $a = 90\ s^{-1}$ at different equivalence ratios: (a) $\Phi = 1.65$; (b) $\Phi = 1.85$; (c) $\Phi = 2.20$; (d) $\Phi = 2.65$.

with experimental observations. Measured and predicted profiles of C_2H_2 are plotted in Figs.6(a) to (d). The agreement between experiment and prediction is fair at lower equivalence ratios, but the predicted maximum concentration of C_2H_2 is much higher than the measurement at higher equivalence ratios. This difference is probably due to over-simplified C_2H_2 chemistry employed here. The links of C_2H_2 chemistry to soot inception make it more complicated [14]. In particular, there are indications that additional outlet channels, such as through OH attacks, rate for which are extremely uncertain [14], need to be included. More work is needed to resolve this discrepancy.

NOx Formation

In the present study, concentrations of NOx were not measured by our NOx analyzer because its response to high concentrations of the C_2 species produces false high NOx readings [8]. Work is continuing to enable reliable NOx results to be extracted in the presence of these complications, but that work is not yet completed. Despite the absence of these critical experimental tests, the present computation may give insight into the NOx formation mechanism in ethane flames, since the present nitrogen chemistry is reasonably successful in two-stage methane flames [8].

In ethane two-stage flames, both thermal NO formation

$$O + N_2 — NO + N \qquad \text{(R25)}$$

and the proinpt mechanism

$$CH + N_2 — HCN + N \qquad \text{(R26)}$$

are important. The CH radicals are dominantly formed by

$$CH_2 + H — CH + H_2 \qquad \text{(R27)}$$

and

$$CH_2 + OH — CH + H_2O, \qquad \text{(R28)}$$

where the CH_2 is from reaction R24, isomerization of $^*CH_2$ and the reaction $CH_3 + H \rightarrow CH_2 + H_2$. The most important consumption steps for CH species are

$$CH + H_2O — CH_2O + H, \qquad \text{(R29)}$$

$$CH + CO_2 — CHO + CO \qquad \text{(R30)}$$

and

$$CH + O_2 — CHO + O. \qquad \text{(R31)}$$

On the basis of a chemical-kinetic steady-state balance, the CH radical concentration can be approximately calculated by

$$X_{CH} = \frac{(k_{27}X_H + k_{28}X_{OH})X_{CH_2}}{k_{29}X_{H_2O} + k_{30}X_{CO_2} + k_{31}X_{O_2}}. \qquad (3)$$

It is clear from this equation that increasing the concentration of CO_2 and H_2O in the region where CH exists reduces X_{CH} and thus decreases NO_x production rates. Concentrations of CH_2 decrease with increasing equivalence ratio Φ, since the higher premixing means higher concentrations of O_2 and leads to a faster

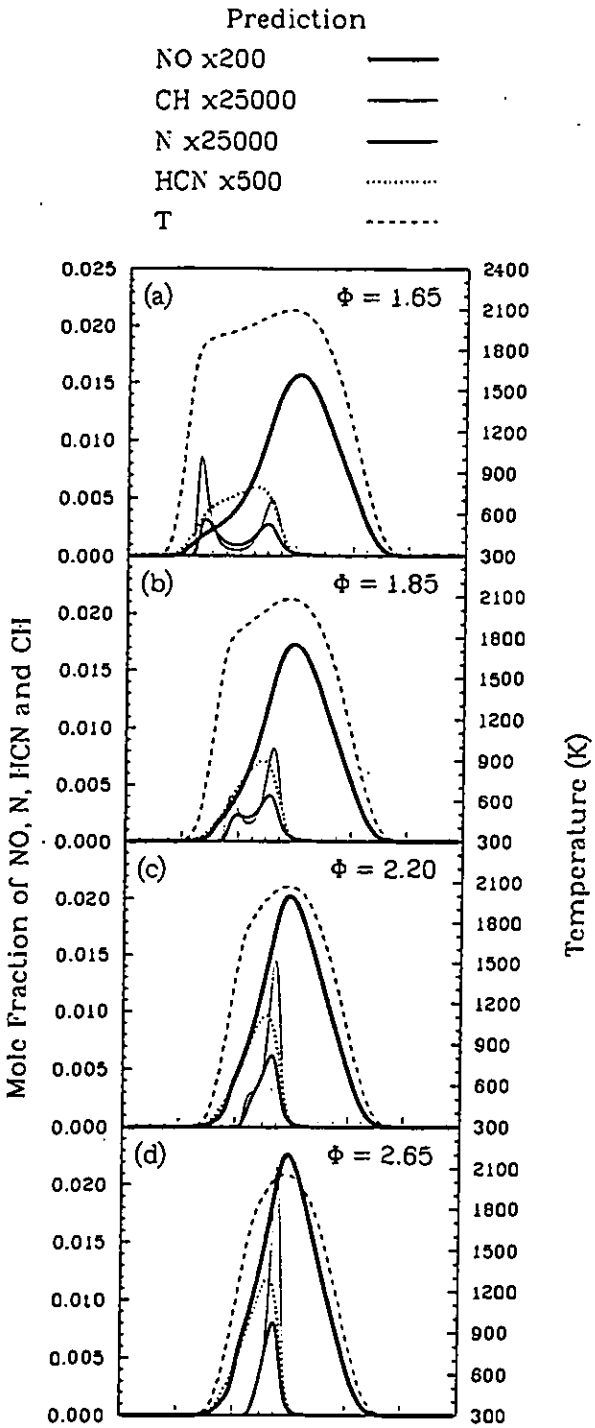

Figure 7: Predicted concentration profiles of NO, CH, N and HCN for strain rate $a = 90\ s^{-1}$ at different equivalence ratios: (a) $\Phi = 1.65$; (b) $\Phi = 1.85$; (c) $\Phi = 2.20$; (d) $\Phi = 2.65$.

consumption rate of CH_2 by reaction R31. In lean premixed flames, the prompt path becomes negligible in comparison with the thermal path because X_{CH_2} is smaller and X_{O_2} is larger, giving a much smaller value of X_{CH} in Eq. 3.

Figure 7 shows calculated concentration profiles of NO, N, HCN and CH. At the lower Φ, as shown in Figs. 7(a) and (b), two CH peaks are predicted as may be expected form Eq. 3 where the concentration profiles of H and OH have two peaks, shown in Figs. 3(a) and (b). This same reason applies to the two peaks of the N radical because N is produced by reactions R25 and R26 and by reactions of NH with H and OH, while it produces NO through reactions of N with OH and O_2. It can be seen from Fig. 7 that the NO concentration reaches its maximum value in the diffusion-flame reaction zone, where the temperature is the highest. Results in Fig. 7 also show that the maximum concentration of NO increases with equivalence ratio; the higher the premixing is, the lower is the NOx formation because of the lower concentrations of HCN and N in the flame. This same type of behavior was observed for methane flames [8], but NOx levels are a little higher for ethane, because of the greater contribution of the prompt mechanism.

CONCLUDING REMARKS

The present work has experimentally and numerically studied the flame chemistry of ethane. Figure 8 shows the principal reaction pathways of ethane oxidation in two-stage combustion with equivalence ratio $\Phi = 1.65$ and strain rate $a = 90\ s^{-1}$ at

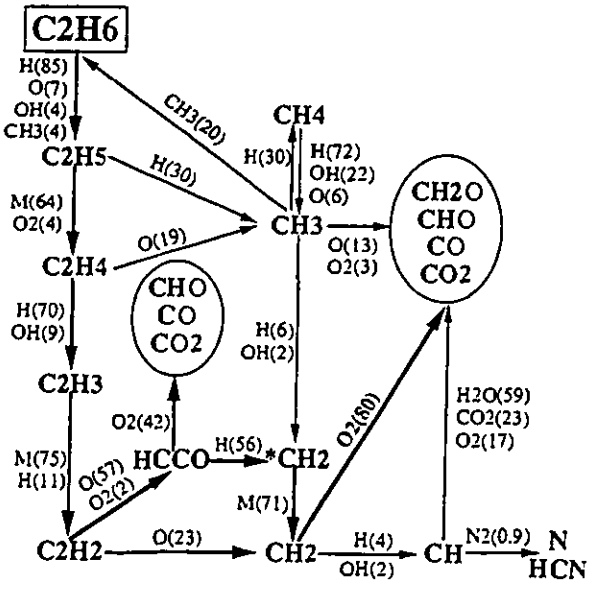

Figure 8: Reaction path for ethane in a two-stage ethane-air flame with equivalence ratio $\Phi = 1.65$ and strain rate $a = 90\ s^{-1}$.

normal atmospheric pressure according to the present results. While specific information in the figure is associated with this condition, the general scheme applies over a wide range of conditions for which two-stage flames exist. In this figure, the heavier arrows represent the main pathways, with the agents and their fractions given in light print. The fractions (in parentheses) are obtained by integrating consumption rates over the entire field, including both flames. Indications of the fates of some of the minor species, such as C_2H, C_3H_3, C_3H_4, and C_3H_6, have been omitted from the diagram for simplicity, although these generally proceed along mainly to the CO_2 and H_2O products. The diagram is designed to track the carbon atom in ethane rather than the hydrogen atoms. The N and HCN, derived from CH, are the sources of prompt NO_x, through subsequent pathways that are not shown.

It is seen here that H plays the most important role in fuel consumption. The important intermediate species are C_2H_5, C_2H_4, C_2H_3, C_2H_2, CH_4, CH_3, *CH2, CH2, HCCO and CH. Because C_2H_4, C_2H_2 and CH_4 are much more stable than other species in flames, their concentrations are high and measurable. The oxidation of radicals CH_2, HCCO, CH_3, CHO and CH_2O leads to CO and CO_2. The radical CH is derived from CH_2 and proceeds to form N and HCN as well as CO and CO_2. Although only less than 1% of the CH is consumed by nitrogen, this is the main source of NO in these flames.

Besides their potential practical interest in increasing combustion stability and reducing pollutant formation, two-stage flames of the kind studied here afford advantages for determining flame chemistry, providing a greater range of reaction-zone conditions and larger distances for easier spatial resolution, thereby aiding in obtaining reliable experimental results. In identifying rate parameters for numerical computations to compare with the present experiments, the previously employed elementary rate data for the reactions $C_2H_4 + H \rightarrow C_2H_3 + H_2$ and $C_2H_4 + OH \rightarrow C_2H_3 + H_2O$ have been modified here to obtained better agreement between experimental measurement and numerical computation.

ACKNOWLEDGMENT

This research was supported by the Department of Energy, Office of Basic Energy Sciences, Division of Engineering and Geosciences under Contract DE-F003-87ER13685.

References

[1] Naber, J.D., Siebers, D.L., Di Julio, S.S. and Westbrook, C.K., "Effects of Natural gas Composition on Ignition Delay under Diesel Conditions," *Combustion and Flame*, 99:192-200 (1994).

[2] Trumpy, D.K., Uyehara, O.A. and Myers, P.S., "The Preknock Kinetics of Ethane in a Spark Ignition Engine," *SAE Tronsactions*, 78:1849-1874 (1969).

[3] Leppard, W.R., "A Detailed Chemical Kinetics Simulation of Engine Knock," *Combustian Science and Technology*, 43:1-20 (1985).

[4] Reisel, J.R., Carter, C.D., Laurendeau, N.M. and Drake, M.C., "Laser-Saturated Fluorescence Measurements of Nitric Oxide in Laminar, Flat, $C_2H_6/O_2/N_2$ Flames at Atmospheric Pressure," *Combustion Science and Technology*, 91:271-295 (1993).

[5] Ravikrishna, R.V. and Laurendeau, N.M., "Brief Communication: Laser-Saturated Fluorescence Measurements of Nitric Oxide in Laminar Counterflow Diffusion Flames," *Combustion and Flame*, 113:473-475 (1998).

[6] Drake, M.C., Ratcliffe, J.W., Blint, R.J., Carter, A.D. and Laurendeau, N.M., "Measurements and Modeling of Flame-front NO Formation and Superequilibrium Radical Concentrations in laminar High-Pressure Premixed Flames," *Twenty-Third Symposium (International) on Combustion*, The Combustion Institute, Pittsburgh, 1990, pp.387-395.

[7] Li, S.C., Ilincic, N. and Williams, F.A., "Reduction of NOx Formation by Water Sprays in Strain Two-Stage Flames," *Journal of Engineering for Gas Turbines and Power*, 119:836 (1997).

[8] Li, S.C. and Williams, F.A., "Experimental and Numerical Studies of NOx Formation in Two-Stage Methane-Air Flames," ASME Paper No. 98-GT-73, 1998.

[9] Smooke, M.D., Seshadri, K. and Puri, I.K., "The structure and Extinction of Partially Premixed Flames Burning Methane in Air," *Twenty-Second Symposium (International) on Combustion*, The Combustion Institute, Pittsburgh, 1988, pp.1555-1563.

[10] Smooke, M.D., Crump, J., Seshadri, K. and Giovangigli, V., "Comparison between Experimental measurements and Numerical Calculations of the Structure of Counterflow, Diluted, Methane-Air, Premixed Flames," *Twenty-Third Symposium (International) on Combustion*, The Combustion Institute, Pittsburgh, 1990, pp.463-470.

[11] Pitsch, H., *Entwicklug eines Programmpaketes zur Berechnung eindimensionaler Flammen am Beispiel einer Gegenstamdiffusionsflamme*. Master thesis, RWTH Aachen, Germany, 1993.

[12] Frenklach, M., Wang, H. and Rabinowitz, M.J., "Optimization and Analysis of Large Chemical Kinetic Mechanism Using The Solution Mapping Method-Combustion of Methane," *Progress in Energy and Combustion Science*, 18:47-73 (1995).

[13] Bhargava, A. and Westmoreland, P.R., "Measured Flame Structure and Kinetics in a Fuel-Rich Ethylene Flame," *Combustion and Flame*, 113:333-347 (1998).

[14] Lindstedt, R.P. and Skevis, G., "Chemistry of Acetylene Flames," *Combustion Science and Technology*, 125:73-137 (1997).